Direct Power Magnitude Control of DFIG-DC System Without Orientation Control

Wu, Chao; Zhou, Dao; Blaabjerg, Frede

Published in:
I E E E Transactions on Industrial Electronics

DOI (link to publication from Publisher):
10.1109/TIE.2020.2970666

Publication date:
2021

Document Version
Accepted author manuscript, peer reviewed version

Direct Power Magnitude Control of DFIG-DC System Without Orientation Control

Chao Wu, *Member, IEEE*, Dao Zhou, *Senior Member, IEEE* and Frede Blaabjerg, *Fellow, IEEE*

***Abstract*—This paper presents a novel direct power magnitude control of DFIG-DC system without orientation control. The stator frequency is directly given and the angle of synchronized *d-q* frame is generated by the integral of stator frequency. The relationship between the stator power and rotor current vector is revealed in this paper. Based on this positive correlation, the output power is easily controlled by the *d*-axis rotor current, and the *q*-axis rotor current is controlled flexible to achieve the smooth switching from no output power to rated power. In accordance with the small signal model, the relationship between decoupling control and coupling control is presented, and the principle to select the reference of *q*-axis rotor current is verified. Furthermore, the improved direct resonant control for torque ripple and harmonic current mitigation can still be applied in this novel control method. Finally, the experiment results are presented to validate the proposed method.**

***Index Terms*— Doubly-fed induction generator, power magnitude control, without orientation control, direct resonant control**

I. Introduction

Along with the fast development of dc mirco grid and the widely used dc networks in the shipboard system and modern aircraft system [1]-[3], there is an urgent need to find an appropriate generator and topology applied in dc grid for dc power generation. As a solution, the doubly fed induction generator (DFIG) connected to dc grid through a diode rectifier on the stator side and low power PWM converter on the rotor side is widely used, because of the low cost, simple structure and flexible control [4]-[5]. This topology is usually named as DFIG-DC system.

Generally, the vector control (VC) strategies with grid voltage orientation are widely employed for grid-connected DFIG through phase locked loop (PLL) [6]-[7]. However, the VC strategies based on grid voltage PLL is unavailable in the DFIG-DC system because there is no ac grid voltage.

Compared with stator voltage, the stator flux contains less harmonic since it is the integral of stator voltage. Thereby, most of the VC strategies applied in DFIG-DC system are based on stator flux orientation control. In [8]-[10], the stator frequency and stator flux angle are obtained based on stator voltage model. In [8]-[9], the stator flux angle is directly calculated based on the arc tangent of stator flux and the stator frequency is obtained by the derivative of stator flux angle, which is highly dependent on the resistance. Furthermore, the stator flux is the integral of stator voltage which is difficult to achieve in practical cases due to the unavoidable dc sampling offset. In [10], the integral block is substituted by inertia link which can reduce the effect of dc sampling offset but not completely eliminate it, which causes fundamental frequency ripple in the orientation angle.

In [11]-[14], the stator frequency and stator flux angle are acquired based on current model. In [11], the magnitude of stator flux is applied for the stator frequency control, which is dependent on the stator inductance and mutual inductance. In [12]-[14], a stator flux PLL is proposed to obtain the stator frequency and stator flux angle by controlling the *q*-axis stator flux to be zero, which can avoid the calculation process but still depends on the ratio of stator inductance and mutual inductance. When the DFIG-DC system is operating in the standalone mode, the dc voltage is also controlled based on the stator flux orientation [15]-[17].

In addition to VC approach, direct power control (DPC) strategies have also been extensively studied for DFIG because of simple power regulation, fast dynamic response and robustness to parameter variations. However, the PLL based on grid voltage is still indispensable for acquiring the orientation angle [18]. In order to avoid the calculation of orientation angle, a direct power control scheme of DFIG without PLL is proposed by using a virtual phase angle which is produced by integrating a fixed angular speed [19]-[20]. However, the stator voltage is still necessary for constructing a transformation matrix, which is not suitable for the DFIG-DC system. On the other hand, the DFIG-DC system has more control freedom such as the stator frequency is not imposed by the ac grid which can be controlled by the speed of rotor current vector.

It should be noted that all existing methods are based on the decoupling control of stator frequency and stator power. In this paper, a novel stator frequency and power control method based on rotor current vector is proposed without orientation control. The angle of synchronous *d-q* frame is directly generated by the integral of stator frequency without orientation control. In this way, the calculating process for obtaining stator frequency or stator flux angle can both be eliminated. Based on revealing the relationship between stator active power and rotor current vector, the stator power can be directly controlled by the *d*-axis rotor current. The *q*-axis rotor current is controlled to be a

Manuscript received October 26, 2019; revised December 26, 2019; accepted January 6, 2020. This work was supported THE VELUX FOUNDATIONS under the VILLUM Investigator Grant REPEPS (Award Ref. No.: 00016591) (*Corresponding author: Dao Zhou*).

Chao Wu, Dao Zhou and Frede Blaabjerg are with the Department of Energy Technology, Aalborg University, Aalborg 9220, Denmark (e-mail: cwu@et.aau.dk, zda@et.aau.dk and fbl@et.aau.dk).

constant value which is employed for switching from no output power to rated output power without changing control strategy.

Furthermore, the principle of selecting the reference of *q*-axis rotor current is elaborated and the relationship between the coupling control and decoupling control is revealed through small signal analysis. When it comes to the torque ripple and harmonic currents, the improved direct resonant control can still be applied when choosing appropriated reference of *q*-axis rotor current, which is also verified by theory analysis and experimental results [21].

The advantages of this novel direct power magnitude control method can be summarized as:

1. The stator frequency control is not dependent on inductance parameters and the dc sampling effect is eliminated.

2. The control strategy can go through from the rated power to no output power without changing the control structure.

3. The relationship between coupling control and decoupling control is revealed and the direct resonant control can still be applied.

This paper is organized as follows. The system configuration and mathematical model is described in section II. The control strategy of DFIG-DC system is elaborated in detail in section III. Furthermore, the performance analysis of proposed control strategy is presented in section IV. Section V shows the experimental results and the conclusion is drawn in section VI.

II. System Configuration and Mathematical Model

A. System Configuration

The DFIG-DC system topology can be seen in Fig. 1, where the rotor side converter (RSC) and stator side diode bridge are connected to a common dc link. The working principle of DFIG providing power to DC grid can be elaborated as: firstly, the rotor side exciting current is injected to rotor winding through the RSC, then the air gap electromotive force (EMF) is established. When the peak value of the phase-phase air gap EMF is higher than dc voltage, the diode bridge conducts and the DFIG transfers power to dc grid.

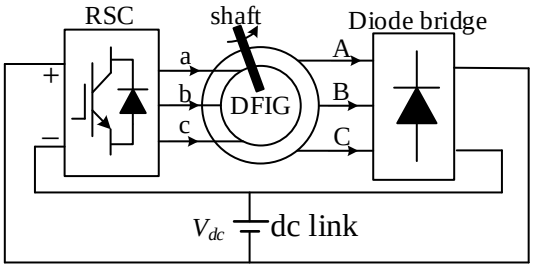

Fig. 1. Configuration of DFIG-DC system.

B. Mathematical Model

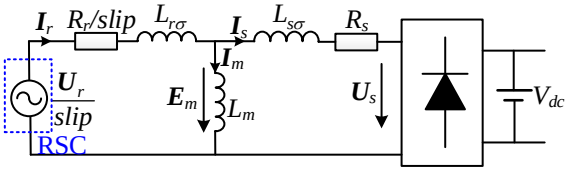

Fig. 2. Steady-state equivalent circuit of the DFIG-DC system.

The steady state phasor equivalent circuit is shown as Fig. 2 [13], where the rotor voltage generated by RSC is transformed to stator side by dividing the slip rate, which is represented by *slip*. $\boldsymbol{I}_s$, $\boldsymbol{I}_r$ and $\boldsymbol{I}_m$ represent the stator, rotor and exciting current, respectively. $\boldsymbol{U}_s$, $\boldsymbol{E}_m$ and $\boldsymbol{U}_r$ represent the stator, air gap and rotor voltage, L_m, $L_{s\sigma}$ and $L_{r\sigma}$ represent the mutual inductance, stator and rotor leakage inductance, R_s and R_r represent the stator and rotor resistance, and V_{dc} is the dc voltage.

The stator voltage and air gap voltage can be expressed as,

$$\begin{cases} \boldsymbol{U}_s = -R_s\boldsymbol{I}_s - jL_{s\sigma}\omega_s\boldsymbol{I}_s + \boldsymbol{E}_m \\ \boldsymbol{E}_m = j\omega_s L_m \boldsymbol{I}_m \end{cases} \tag{1}$$

where ω_s is the stator angular frequency.

According to the equivalent circuit, the relationship between stator current and rotor current can be expressed as,

$$\boldsymbol{I}_r = \boldsymbol{I}_s + \boldsymbol{I}_m \tag{2}$$

Compared with the stator leakage inductance, the stator resistance is much smaller, it can be ignored. Thus, the air gap voltage can be calculated as,

$$\boldsymbol{E}_m = \boldsymbol{U}_s + j\omega_s L_{s\sigma}\boldsymbol{I}_s \tag{3}$$

The stator current is in the same phase with stator voltage due to characteristic of diode bridge [12], so the phasor diagram of steady-state can be illustrated as Fig. 3, where γ is the angle between rotor current and *d*-axis, δ is the angle between stator voltage and rotor current, η is the angle between stator voltage and *d*-axis.

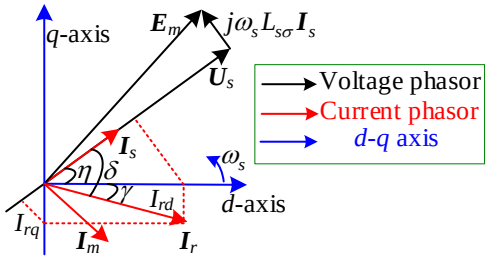

Fig. 3. Phasor diagram of DFIG in steady-state operation.

The torque can be expressed by stator and rotor current as,

$$T_e = L_m\left(\boldsymbol{I}_s \times \boldsymbol{I}_r\right) = L_m\left(I_{rd}I_{sq} - I_{rq}I_{sd}\right) \tag{4}$$

Since the stator current and stator voltage are in phase, the stator power can be calculated by stator voltage and current as,

$$P_s = R_e\left(\boldsymbol{U}_s \cdot \boldsymbol{I}_s\right) = \left|\boldsymbol{U}_s\right|\left|\boldsymbol{I}_s\right| \tag{5}$$

where $\left|\boldsymbol{U}_s\right|$ is the magnitude of stator voltage, $\left|\boldsymbol{I}_s\right|$ is the magnitude of stator current.

The angle between rotor current and *d*-axis can be expressed as,

$$\gamma = \arctan\left(\frac{I_{rq}}{I_{rd}}\right) \tag{6}$$

It should be noted that this angle may become negative when the ratio is negative in (6).

According to (1), (2), and (5), the rotor current can be expressed as,

$$\boldsymbol{I}_r = \boldsymbol{I}_s + \frac{\boldsymbol{U}_s + j\omega_s L_{s\sigma}\boldsymbol{I}_s}{j\omega_s L_m} = \frac{L_s}{L_m}\boldsymbol{I}_s + \frac{\boldsymbol{U}_s}{j\omega_s L_m} = \frac{L_s}{L_m}\frac{P_s}{|\boldsymbol{U}_s|^2}\boldsymbol{U}_s - j\frac{\boldsymbol{U}_s}{\omega_s L_m} \tag{7}$$

where L_s is the stator inductance, which is the sum of L_m and $L_{s\sigma}$

Since the two terms in (7) are orthogonal relationship, the phase angle between stator voltage and rotor current can be calculated as,

$$\delta = \arctan\left(\frac{|\boldsymbol{U}_s|^2}{\omega_s L_s P_s}\right) \tag{8}$$

The angle between stator voltage and d-axis is the sum of δ and γ as,

$$\eta = \arctan(\frac{I_{rq}}{I_{rd}}) + \arctan\left(\frac{|\boldsymbol{U}_s|^2}{\omega_s L_s P_s}\right) \tag{9}$$

The magnitude of stator current can be expressed as,

$$|\boldsymbol{I}_s| = \frac{L_m}{L_s}\left(I_{rd}\cos\eta + I_{rq}\sin\eta\right) \tag{10}$$

According to (6) and (10), the relationship between stator power and rotor current and can be expressed as,

$$P_s = \frac{L_m}{L_s}|\boldsymbol{U}_s|\left(I_{rd}\cos\eta + I_{rq}\sin\eta\right) \tag{11}$$

The relationship expressed in (11) is the foundation of the direct power magnitude control and this will be elaborated in detail in section III and IV.

III. Control Strategy

Since the dc voltage is constant, the control objective of RSC is to achieve accurate regulation of output power to dc grid. Furthermore, the stator frequency of DFIG is not imposed by ac grid, which also needs to be controlled additionally.

The RSC control scheme for the regulation of stator power and stator frequency is shown as Fig. 4, which mainly consists of the stator frequency control, the stator power control and the reference of q-axis rotor current. The stator frequency control block is applied to generate the angle for synchronous d-q frame. The active power control is applied for generating the reference of d-axis rotor current. The reference of q-axis rotor current is applied for supporting the stator voltage when there is no output power to dc side. The stator frequency control, stator power control, reference of q-axis rotor current will be elaborated in detail in the following three parts.

A. Stator frequency control

In steady state, the stator frequency is determined by the rotating speed of rotor current vector. Since there is no orientation control used in this paper, the angle of synchronous d-q frame can be directly set as the integral of stator frequency. The stator frequency is given as ω_s and the angle of synchronous d-q frame is obtained by integrating stator frequency as,

$$\theta_s = \frac{1}{s}\omega_s \tag{12}$$

The angle for Park transformation of rotor voltage and current can be expressed as,

$$\theta_{slip} = \frac{1}{s}\omega_s - \theta_r \tag{13}$$

Thereby, both the stator frequency and angle of synchronous d-q frame are directly given without any additional control, which means the current control has no effect on the stator frequency. Compared with other stator frequency control methods, this method is more stable and simpler.

B. Stator power control

As it can be seen from (11), the stator active power is related with the d-axis rotor current, the power can be regulated through the d-axis rotor current. Thus, the generation of d-axis rotor current can be expressed as,

$$I_{rd}^* = \frac{k_{pp}s + k_{ip}}{s}\left(P_s^* - P_s\right) \tag{14}$$

where k_{pp} and k_{ip} are the proportional and integral gain of the stator power controller.

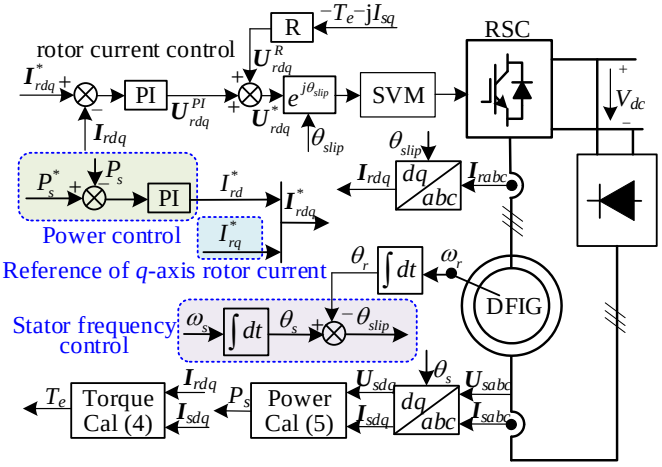

Fig. 4. RSC control scheme for stator frequency and power regulation.

C. Reference of q-axis rotor current

As can be seen from Fig. 4, the reference of q-axis rotor current is adjustable, which can be used to build stator voltage during no output power.

In the case of no output power, the phase to phase voltage of air gap EMF should be smaller than the dc voltage, thereby,

$$|\boldsymbol{E}_m| = \left|\omega_s L_m I_{rq}^*\right| \le V_{dc}/\sqrt{3} \tag{15}$$

In order to simplify the expression of q-axis rotor current, the variables in (15) are all standardized to per unit. The base value of stator voltage is $V_{dc}/\sqrt{3}$ and the base value of stator frequency is 50 Hz. The stator frequency is usually set as 50Hz. Thus, the range of q-axis rotor current in per unit can be expressed as,

$$-1/L_m \le I_{rq}^* \le 1/L_m \tag{16}$$

The reference of q-axis rotor current can be classified into three categories: positive, zero and negative. In order to analyze the effect of q-axis rotor current, three different value of q-axis rotor current are analyzed in detail.

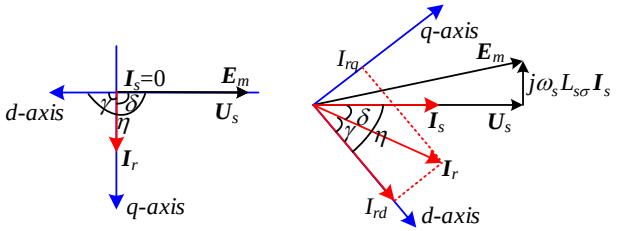

Fig. 5. Phasor diagram of positive q-axis rotor current.

If the q-axis rotor current reference is positive, the relationship of the phasor diagram and the d-q axis can be shown in Fig. 5, where the reference of I_{rq} is $1/L_m$. As seen from Fig. 5, the angle η is almost 180° when the stator output power is zero. With the increase of stator output power, both the angle δ and γ decrease due to the higher d-axis rotor current and the constant q-axis rotor current. Thereby, the range of angle η is between 0° and 180° under this circumstance.

If the q-axis rotor current reference is zero, the relationship between the phasor diagram and the d-q axis can be shown in Fig. 6, which is actually a rotor current orientation. Thus, the angle η is always the same with the angle δ. It is noted that when the stator output power is zero, the angle η is 90° since there is no active current. When the stator output power is 1 pu, the angle η is smaller than 90°, which can be calculated by (8). In conclusion, the range of angle η is between 0° and 90°, and it decreases with the increase of stator output power.

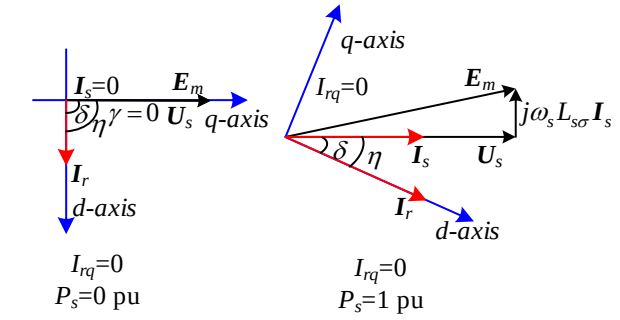

Fig. 6. Phasor diagram of zero q-axis rotor current.

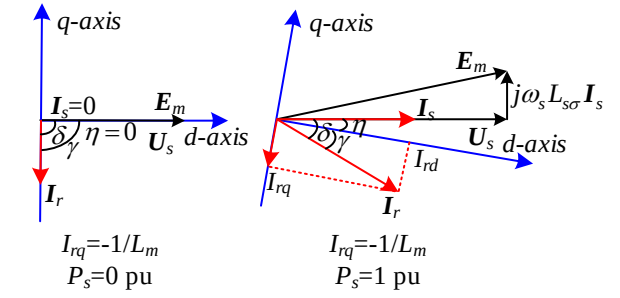

Fig. 7. Phasor diagram of negative q-axis rotor current.

If the reference of q-axis rotor current is negative, the relationship between the phasor diagram and the d-q axis can be shown in Fig. 7, where the reference of I_{rq} is -1/L_m, which is almost a stator voltage orientation method. Since the q-axis rotor current is negative and d-axis rotor current is always positive, the angle γ calculated from (6) is negative. When the stator output power is zero, the angle γ is nearly -90°. Thus, the angle η is almost zero. With the increase of stator output power, the exciting current becomes larger due to the voltage drop on stator leakage inductance. Thus, the angle η will be larger but near zero, which implies that this is almost the same as the stator voltage orientated control.

The change of angle η with different q-axis rotor current and stator output power based on (9) is shown in Fig. 8. In Fig. 8, the stator power changes from 0.2 pu to 1 pu, the angle η decreases which is corresponding with the analysis in Fig. 5 , Fig. 6 and Fig. 7. It demonstrates that I_{rq}=-1/L_m has the best performance since the angle η is almost equal to zero which is just like a stator voltage orientation control.

The change of I_{rd} with different q-axis rotor current and stator output power is shown in Fig. 9. Consistent with Fig. 8, the stator power changes from 0.2 pu to 1 pu, the I_{rd} increases with the power. The I_{rd} is much larger when I_{rq}=0 since the exciting current is also contained in I_{rd} in this condition. The I_{rd} is almost the same when I_{rq} = ±1/L_m since the magnitude of rotor current is the same under a given power.

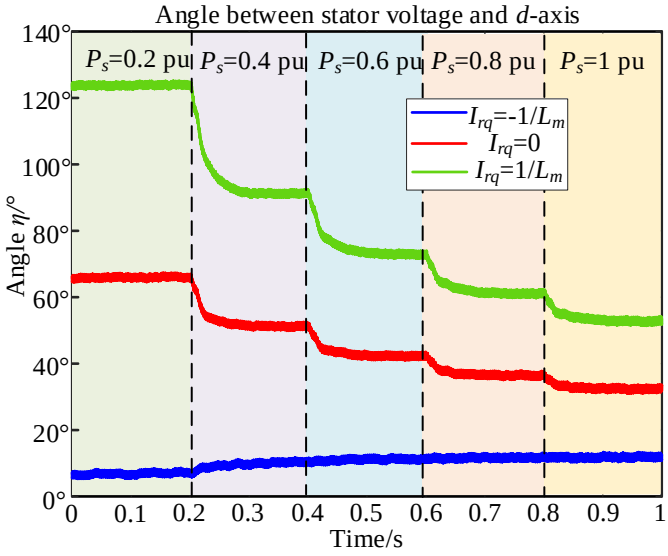

Fig. 8. Change of angle η with different I_{rq} and P_s.

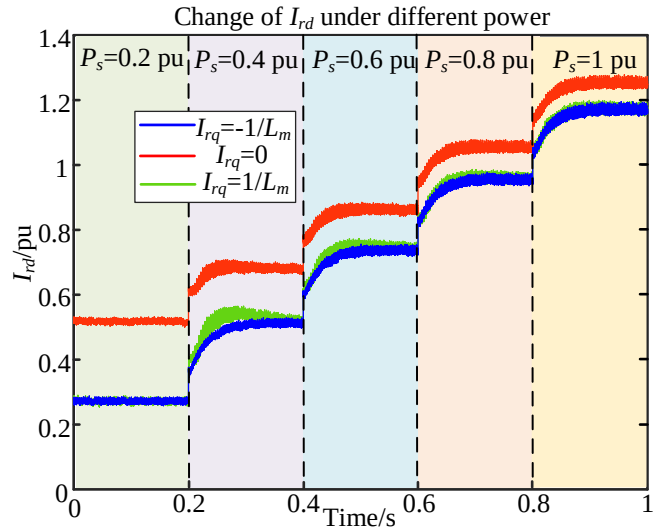

Fig. 9. Change of I_{rd} with different I_{rq} and P_s.

Thus, in order to get an appropriate stator voltage when there

is no power and to achieve an almost stator voltage orientation, the reference of *q*-axis rotor current is preferred as,

$$I_{rq}^{*} = -1/L_m \tag{17}$$

IV. Control Performance Analysis

As can be seen from the power expression in (11), the stator output power is not only related with I_{rd} but also related to I_{rq} and angle η. The reference of I_{rq} is a fixed value and the rotor current control loop is faster than the power loop, the I_{rq} can be considered as a constant value. The angle η is a changing angle which is determined by the P_s and I_{rd}. Thus, the relationship between stator power and *d*-axis rotor current is non-linear. In order to analyze the control performance of power loop, a small signal model based on (11) should be built. In this section, the small signal model of the direct power magnitude control loop is deduced. The dynamic performance of coupling control and decoupling control are compared based on this model. Furthermore, the harmonic currents and torque ripple which are caused by distorted stator voltage are analyzed and the improved direct resonant control is introduced to mitigate torque ripple and harmonic currents.

A. Performance of direct power magnitude control

As can be seen from (11), the stator power is related with both *d*-axis rotor current and angle η, which is not linear. The relationship between the stator active power and *d*-axis rotor current and angle η can be expressed by the derivative as,

$$\frac{\partial P_s}{\partial I_{rd}} = \frac{L_m}{L_s}|\boldsymbol{U}_s|\cos\eta \tag{18}$$

$$\frac{\partial P_s}{\partial \eta} = \frac{L_m}{L_s}|\boldsymbol{U}_s|\left(-I_{rd}\sin\eta + I_{rq}\cos\eta\right) = -\frac{L_m}{L_s}|\boldsymbol{U}_s||\boldsymbol{I}_r|\sin\delta \tag{19}$$

where $|\boldsymbol{I}_r|$ is the magnitude of rotor current.

As can be seen from (9), the angle η is determined by *d*-axis rotor current and stator power. The effect of rotor current and stator power on the angle η can also be obtained by the partial derivative as,

$$\frac{\partial \eta}{\partial I_{rd}} = \frac{-I_{rq}}{I_{rd}^2 + I_{rq}^2} \tag{20}$$

$$\frac{\partial \eta}{\partial P_s} = \frac{-|\boldsymbol{U}_s| I_{ms}}{P_s^2 + \left(|\boldsymbol{U}_s| I_{ms}\right)^2} \tag{21}$$

where I_{ms} is equal to $|\boldsymbol{U}_s|/L_s$.

Under the steady-state, assuming the stator power is P_{s0}, *d*-axis rotor current is I_{rd0} and the three angles are γ_0, δ_0, η_0, respectively. Thus, the block diagram of power loop control can be deduced as Fig. 10. Since the rotor current control loop is much faster than the power control loop, the rotor current control loop is equivalent as a unity block.

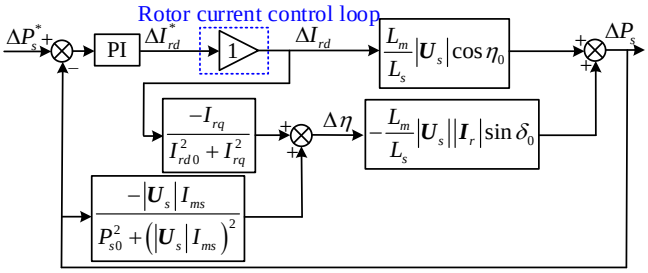

Fig. 10. Transfer function block diagram of power control loop.

Based on the relationship between the three angles, the transfer function block diagram of power control loop can be simplified as Fig. 11.

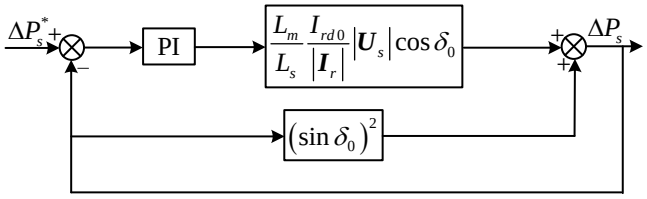

Fig. 11. Simplified block diagram of power control loop.

As can be seen from Fig. 11, the open loop transfer function can be expressed as,

$$G_{open}(s) = \frac{L_m}{L_s} G_{PI}(s)|\boldsymbol{U}_s|\frac{\cos\gamma_0}{\cos\delta_0} \tag{22}$$

As can be seen from the open loop transfer function, if $\cos\gamma_0$ is equal to $\cos\delta_0$, which means angle η is zero and this condition is just equal as stator voltage orientation control. If $\cos\gamma_0$ is bigger than $\cos\delta_0$, the coupling control has a better dynamic performance than decoupling control with same PI parameters. For a given stator power, δ_0 is a constant value which can be acquired by (8). The maximum value of $\cos\gamma_0$ is 1, which means γ_0 is equal to zero. This is just the rotor current orientation control. It proves that the rotor current orientation control has the fastest dynamic performance among all the decoupling control methods.

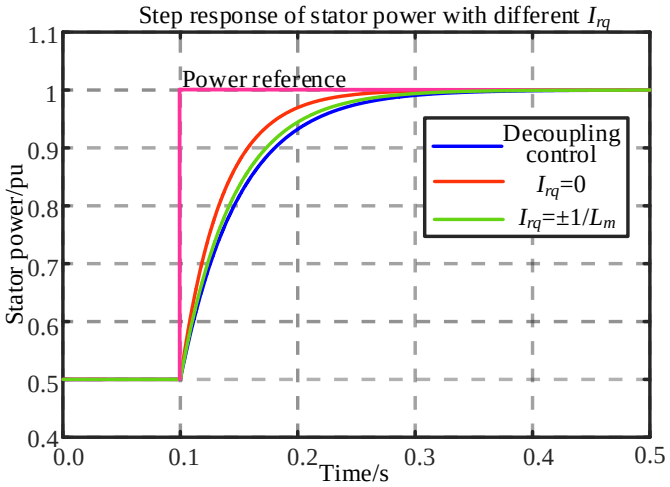

Fig. 12. Step response of stator power with different I_{rq}.

According to the transfer function block diagram shown in Fig. 10, the step response of stator power with different I_{rq} is shown in Fig. 12. At the beginning, the power reference is 0.5 pu

which is a steady-state operation. At 0.1s, the power reference changes to 1 pu, the dynamic performance is different with different *q*-axis rotor current. When I_{rq}=0, the power response is most quick since the *d*-axis rotor current is higher than the active current. When $I_{rq}=\pm 1/L_m$, the power response is the same, which are also near the response of decoupling control since the *q*-axis rotor current is almost the same with true exciting current. Thus, the performance of power magnitude control is almost the same as decoupling control when I_{rq}=-1/L_m.

B. Effectiveness of direct resonant control

As discussed before, only the fundamental current and average power are analyzed in Section V(A). The torque ripple and harmonic current are not analyzed and the strategy for torque ripple mitigation in the coupling control should be studied. In the decoupling control method, direct resonant control is a simple and effective method in mitigating torque ripple and harmonic currents [21]. However, whether the direct resonant control is still applicable in the coupling control should be analyzed.

Since the main harmonic component in the stator voltage is 5th and 7th order harmonic, only the 6th order harmonic current and torque ripple are considered. When considering the 6th order harmonic current in both stator and rotor current in the synchronous *d-q* frame, the torque in (4) can be rewritten as,

$$T_e=L_m\left(\left(I_{rd0}+I_{rd6}\right)\left(I_{sq0}+I_{sq6}\right)-\left(I_{rq0}+I_{rq6}\right)\left(I_{sd0}+I_{sd6}\right)\right) \quad (23)$$

where I_{rd0}, I_{rq0}, I_{sd0}, I_{sq0} represent the rotor and stator fundament current in *d-q* axis, I_{rd6}, I_{rq6}, I_{sd6}, I_{sq6} represent the rotor and stator harmonic current in *d-q* axis.

Since the direct power magnitude control is a coupling control method, the rotor and stator fundamental current in *d-q* axis are not zero. The torque expression in (23) can not be simplified, the 6th order torque ripple can be expressed as,

$$T_{e6}=L_m\left(I_{rd0}I_{sq6}+I_{sq0}I_{rd6}-I_{rq0}I_{sd6}-I_{sd0}I_{rq6}\right) \quad (24)$$

When there is no harmonic voltage injected in the rotor side to reduce the harmonic current, the harmonic currents in the rotor and stator side are almost the same because the mutual inductance is equivalent to short circuit for harmonic current [13]. Thus, the 6th order torque ripple can be simplified as,

$$T_{e6}=L_m\left(\left(I_{sq0}-I_{rq0}\right)I_{rd6}+\left(I_{rd0}-I_{sd0}\right)I_{rq6}\right) \quad (25)$$

The advantage of the direct resonant control is that only one axis is enough for mitigating the torque ripple and the other axis can be used for reducing harmonic current [21]. Thus, the direct resonant control is also expected to be used in this coupling control method. The key principle of the direct resonant control is that the coefficient of rotor harmonic current is not zero and always is a determinate direction.

As it can be seen from (25), the two coefficients of *d-q* axis rotor harmonic current are neither zero, which means the torque ripple may be mitigated in any axis. However, the *d*-axis rotor current is almost the same with *d*-axis stator current when it is almost stator voltage orientation which can be seen in Fig. 8. Therefore, the *q*-axis rotor harmonic current is not suitable for mitigating the torque ripple. On the other hand, the coefficient of *d*-axis rotor harmonic current is always positive and almost equal to 1/L_m, which is suitable for mitigating the torque ripple. Thus, *d*-axis is applied for mitigating torque ripple and *q*-axis is applied for mitigating harmonic current.

The transfer function of the resonant controller used in this paper can be expressed as,

$$G_R(s)=\frac{2k_r\omega_c s}{s^2+2\omega_c s+(6\omega_s)^2} \quad (26)$$

where ω_c is the cutoff frequency and k_r is the gain of the resonant controller.

The rotor voltage for mitigating torque ripple and harmonic currents can be expressed as,

$$\boldsymbol{U}_{rdq}^{R}=G_R(s)\left(0-T_e\right)+jG_R(s)\left(0-I_{sq}\right) \quad (27)$$

The equation (27) indicates that the harmonic reference for torque and *q*-axis stator are both set as zero.

Finally, the rotor voltage reference can be expressed as,

$$\boldsymbol{U}_{rdq}^{*}=\boldsymbol{U}_{rdq}^{PI}+\boldsymbol{U}_{rdq}^{R} \quad (28)$$

where $\boldsymbol{U}_{rdq}^{PI}$ is the output of the PI controller, $\boldsymbol{U}_{rdq}^{R}$ is the output of the direct resonant control.

V. Experimental Validation

In order to validate the control strategy proposed in section III, a DFIG-based experimental system is developed. The schematic diagram of the experimental system is shown in Fig. 13. The DFIG was driven by a squirrel cage induction motor with the control of general inverter. The control strategy of the RSC is implemented on the TI DSP TMS320F28335 and the switching frequency is 10 kHz with a sampling frequency of 10 kHz. The parameters of the DFIG are shown in Table I. All the waveforms are acquired by a YOKOGAWA DL750 scope.

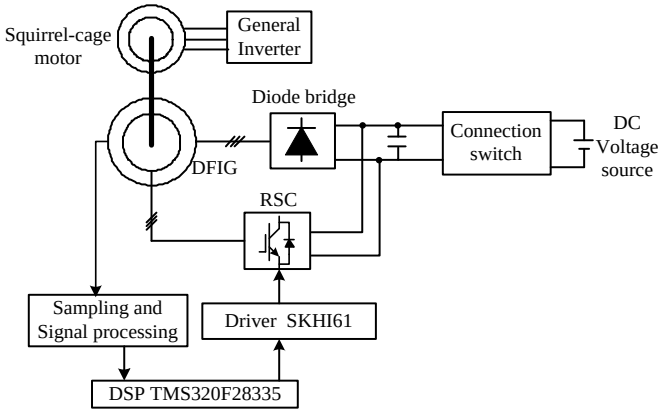

Fig. 13. Schematic diagram of the experimental system.

TABLE I Parameters of the tested DFIG-DC system

Parameters	*Value*	*Parameters*	*Value*
Rated power	1.0 kW	Rated voltage	110 V
Rated frequency	50 Hz	DC voltage	140 V
Pole pairs	3	R_s	1.01 Ω
R_r	0.88 Ω	L_m	87.5 mH
$L_{\sigma s}$	5.6 mH	$L_{\sigma r}$	5.6 mH

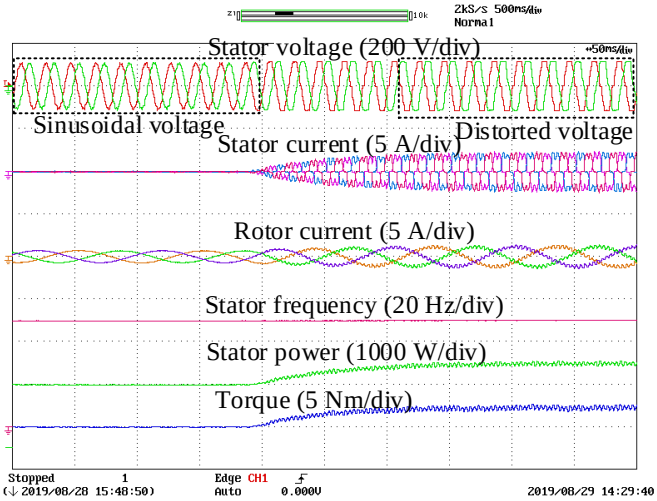

Fig. 14. Experimental results from no output power to 400 W output power.

Fig. 14 shows the experimental results of DFIG from zero output power to 400 W. The stator frequency is set as 50 Hz and the rotor speed is 800 rpm. At the beginning, the stator output power is set as zero and the q-axis rotor current is $-1/L_m$, which is used to build the stator side voltage. As can be seen from the experimental results, the stator voltage and rotor current are both sinusoidal when the diode bridge does not conduct without any power transmission from stator side. When the stator output power is set as 400 W, the diode bridge conducts and stator current increases. With the increase of stator output power, the stator voltage is gradually distorted, the stator current and rotor current both contain low order harmonics which also cause torque and power ripples.

Fig. 15 shows the experimental results of DFIG when the stator output power changes from 400 W to 0 W. As can be seen from the experimental results, the stator current gradually decreases to be zero when the output power reference is zero. During this dynamic period, both stator voltage and rotor current are very stable without any fluctuation, which means that this direct power magnitude control method can go through zero output power without changing control strategy.

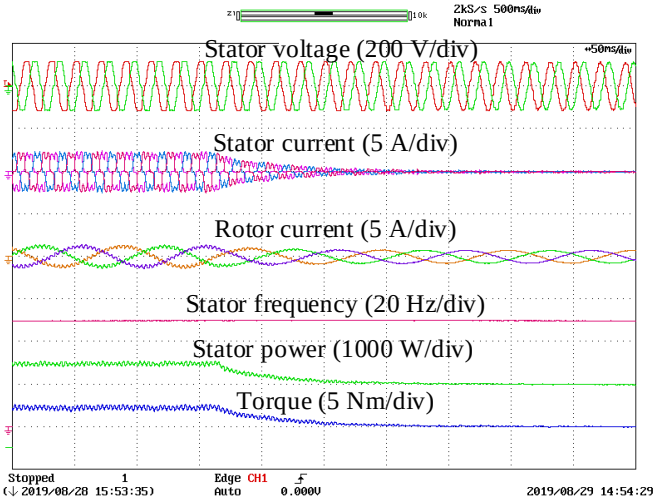

Fig. 15. Experimental results from 400 W output power to no output power.

Fig. 16 shows the step response of DFIG when the stator active power reference changes from 100 W to 800 W. The rotor speed is 800 rpm and the stator frequency is set as 50 Hz. The change of stator power has no effect on the stator frequency. The stator active power can track the power reference accurately in 150 ms without any overshoot since the power control loop is just a first order system, which is corresponding with the theoretical analysis in part A section IV.

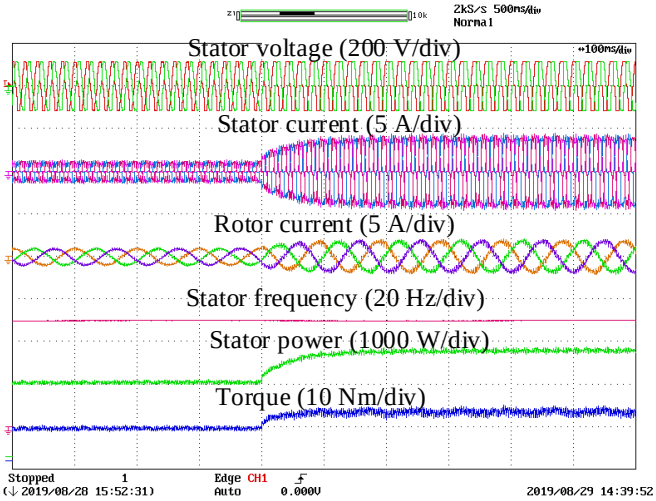

Fig. 16. Step response of power change from 100W to 800W.

The step response of the stator frequency change from 50 Hz to 60 Hz is shown in Fig. 17. The stator power reference is 500 W. During the change of stator frequency, the stator power has a pulsation which is caused by transient stator flux but will come to steady state in 60 ms. Compared with other stator frequency control method, the stator frequency is direct given without any dynamic response which is more stable and robust.

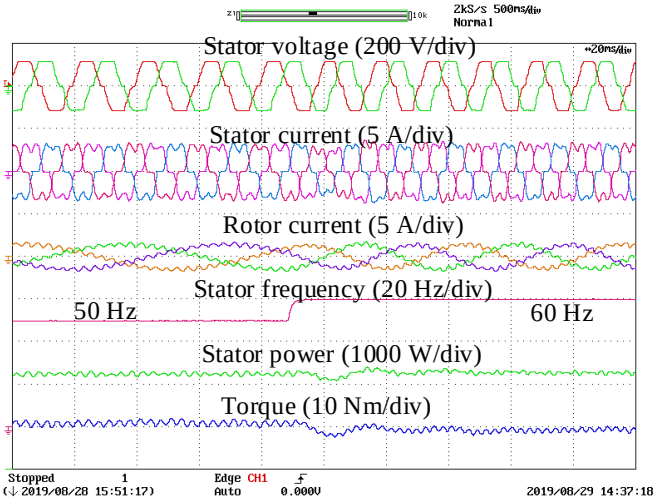

Fig. 17. Step response of stator frequency change from 50 Hz to 60 Hz.

Fig. 18 shows the steady experimental results of DFIG when the stator power reference is 500 W and stator frequency is 50 Hz. Due to the diode bridge on the stator side, the stator current is highly distorted with 5^{th} and 7^{th} order harmonics, which are 24.6% and 3.9%, respectively. The 300 Hz ripples in the torque is 6.5%, which is harmful for the mechanical shaft of DFIG. The 6^{th} order harmonic in q-axis stator current is also very obvious which increases the current loss of the DFIG-DC system.

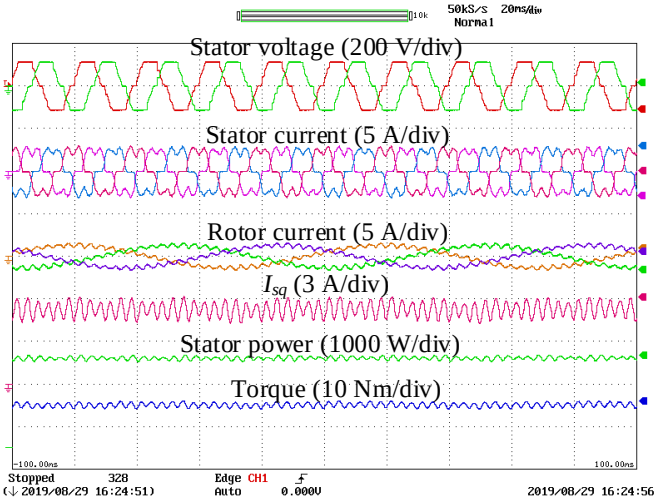

Fig. 18. Steady state experimental results of DFIG-DC system.

Fig. 19 shows the experimental results of DFIG with direct resonant control. The stator power reference and stator frequency are the same as Fig. 18. The direct resonant control is applied for mitigating the torque ripple and *q*-axis stator harmonic current. As can be seen from this figure, the ripples in torque and *q*-axis stator current have been greatly reduced, which validates the effectiveness of direct resonant control in this coupling control method. However, the stator current is not so sinusoidal as [21] because it is not a ideal voltage orientation method, which may cause more harmonic currents in mitigating the torque ripple. The performance of torque ripple mitigation is the same with other decoupling control methods.

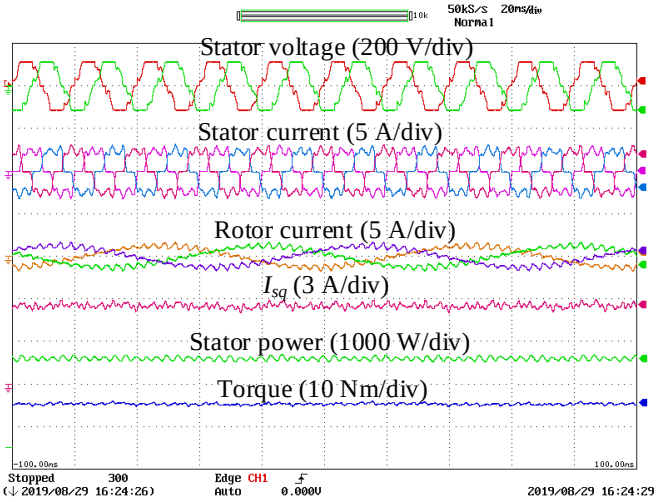

Fig. 19. Experimental results of DFIG with direct resonant control.

VI. Conclusion

A novel direct power magnitude control method for DFIG-DC system is proposed based on a given stator frequency and angle of synchronous *d*-*q* frame. The *d*-axis rotor current is used to regulate the stator power and the *q*-axis rotor current is used to generate stator voltage. In this way, the control strategy is able to go through from no output power to rated output power without changing the control strategy. The effect of different *q*-axis rotor current is investigated and it is proved that the dynamic performance of coupling control is better than the decoupling control by the small signal analysis. Since the stator power control loop is a first order system, the dynamic performance can be designed fast without any overshoot. Furthermore, the direct resonant control for reducing the torque ripple and harmonic current can still be applied in the power magnitude control. Thus, the efficiency can be improved by reducing the harmonic current losses. In conclusion, both the fundamental and harmonic current regulation are effective through the power magnitude control, which is a highly stable and robust control method for DFIG-DC system.

In this paper, the dc voltage is assumed constant and the DFIG is working as a power source. However, the dc voltage is not constant in some case. Thus, the control strategy for stand-alone DFIG-DC system should also be investigated in the future work, which can go through both the grid-connected and standalone condition.

References

[1] T. Dragicevic, X. Lu, J. C. Vasquez, and J. M. Guerrero, "DC microgrids— Part I: A review of control strategies and stabilization techniques," *IEEE Trans. Power Electron.*, vol. 31, no. 7, pp. 4876–4891, Jul. 2016.

[2] Z. Jin, G. Sulligoi, R. Cuzner, L. Meng, J. C. Vasquez, and J. M. Guerrero, "Next-generation shipboard DC power system: Introduction smart grid and dc microgrid technologies into maritime electrical netowrks," *IEEE Electrific. Mag.*, vol. 4, no. 2, pp. 45–57, Jun. 2016.

[3] Q. Xu, Y. Xu, P. Tu, T. Zhao and P. Wang, "Systematic reliability modeling and evaluation for on-board power systems of more electric aircrafts," *IEEE Trans. Power Syst.*, vol. 34, no. 4, pp. 3264-3273, Jul. 2019.

[4] G. D. Marques and M. F. Iacchetti, "DFIG topologies for DC networks: A review on control and design Features," *IEEE Trans. Power Electron*, vol. 34, no. 2, pp. 1299-1316, Feb. 2019.

[5] H. Nian and X. Yi, "Coordinated control strategy for doubly-fed inductiongenerator with dc connection topology," *IET Renew. Power Gener.*, vol. 9,no. 7, pp. 747–756, Aug. 2015.

[6] C. Liu, F. Blaabjerg, W. Chen, and D. Xu, "Stator current harmonic control with resonant controller for doubly fed induction generator," *IEEE Trans. Power Electron.*, vol. 27, no. 7, pp. 3207–3220, Jul. 2012.

[7] J. Hu, H. Nian and H. Xu, et al., "Dynamic modeling and improved control of DFIG under distorted grid voltage conditions," *IEEE Trans. Energy Convers.*, vol.26, no.1, pp. 163-175, Mar. 2011.

[8] G. D. Marques, M. F. Iacchetti, "Stator frequency regulation in a field oriented controlled DFIG connected to a DC Link," *IEEE Trans. Ind Electron.*, vol. 61, no. 11, pp. 5930-5939, Nov. 2014.

[9] G. D. Marques, M. F. Iacchetti, "Inner control method and frequency regulation of a DFIG connected to a DC link," *IEEE Trans. Energy Convers.*, vol.29, no.2, pp.435-444, Jun. 2014.

[10] M. F. Iacchetti, G. D. Marques, and Roberto Perini, "Torque ripple reduction in a DFIG-DC system by resonant current controllers," *IEEE Trans. Power Electron.*, vol.30, no.8, pp. 4244-4254, Aug. 2015.

[11] H. Nian, C. Wu, and P. Cheng, "Direct resonant control strategy for torque ripple mitigation of DFIG connected to DC link through diode rectifier on stator," *IEEE Trans. Power Electron.*, vol. 32, no. 9, pp. 6936–6945, Sep. 2017.

[12] G. D. Marques, M. F. Iacchetti, "A self-sensing stator-current-based control system of a DFIG connected to DC-link", *IEEE Trans. Ind Electron.*, vol. 62, no. 10, pp. 6140-6150, Oct. 2015.

[13] C. Wu and H. Nian, "Sinusoidal current operation of DFIG-DC System without stator voltage sensors," *IEEE Trans. Ind. Electron.*, vol. 65, no. 8, pp. 6250–6258, Aug. 2018

[14] C. Wu, H. Nian, "An improved repetitive control of DFIG-DC system for torque ripple suppression," *IEEE Trans. on Power Electron.*, vol. 33, no.9, pp. 7634-7644, Sep. 2018.

[15] H. Misra, A. Gundavarapu, and A. K. Jain, "Control scheme for DC voltage regulation of stand-alone DFIG-DC system," *IEEE Trans. Ind. Electron.*, vol. 64, no. 4, pp. 2700–2708, Apr. 2017.

[16] H. Misra and A. K. Jain, "Analysis of stand alone DFIG-DC system and DC voltage regulation with reduced sensors," *IEEE Trans Ind. Electron.*, vol. 64, no. 6, pp. 4402–4412, Jun. 2017.
[17] H. Misra and A. K. Jain, "Mathematical modelling and control of standalone DFIG-DC system in rotor flux reference frame," *IEEE Trans. Ind.Electron.*, vol. 65, no. 5, pp. 3708–3717, May. 2018.
[18] H. Nian, and Y. P. Song, "Direct power control of doubly fed induction generator under distorted grid voltage," *IEEE Trans. Power Electron.*, vol. 29, no. 2, pp. 894-905, Feb. 2014.
[19] H. Nian, P. Cheng and Z. Q. Zhu, "Coordinated direct power control of DFIG system without phase-locked loop under unbalanced grid voltage conditions," *IEEE Trans. Power Electron*., vol. 31, no. 4, pp.2905-2918, Jul. 2016.
[20] H. Nian, P. Cheng, and Z. Q. Zhu, "Direct power control of doubly fed induction generator without phase-locked loop in synchronous reference frame during frequency variations," *IET Renew. Power Gener.*, vol. 9, no. 6, pp. 576-586, Aug. 2015.
[21] C. Wu and H. Nian, "Improved direct resonant control for suppressing torque ripple and reducing harmonic current losses of DFIG-DC system," *IEEE Trans. Power Electron*, vol. 34, no. 9, pp. 8739-8748, Sep. 2019.

Chao Wu (M'19) was born in Hubei Province, China. He received the B.Eng. degree from HeFei University of Technology, Hefei, China and the Ph.D. degree from Zhejiang University, Hangzhou, China, in 2014 and 2019, both in electrical engineering. He is currently a Postdoctoral Researcher in the Department of Energy Technology, Aalborg University, Aalborg, Denmark.
His current research interests include cooperative control of multi-converter systems, particularly the control and operation of doubly fed induction generators for DC connection.

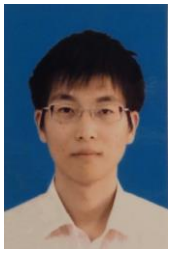

Dao Zhou (S'12-M'15-SM'19) received the B.S. from Beijing Jiaotong University, Beijing, China, in 2007, the M. S. from Zhejiang University, Hangzhou, China, in 2010, and the Ph.D. from Aalborg University, Aalborg, Denmark, in 2014, all in electrical engineering.
Since 2014, he has been with Department of Energy Technology, Aalborg University, where currently he is an Assistant Professor. His research interests include modeling, control, and reliability of power electronics in renewable energy application.
Dr. Zhou received the Renewable and Sustainable Energy Conversion Systems of the IEEE Industry Applications Society First Prize Paper Award in 2015, and Best Session Paper at Annual Conference of the IEEE Industrial Electronics Society (IECON) in Austria in 2013.

Frede Blaabjerg (S'86–M'88–SM'97–F'03) was with ABB-Scandia, Randers, Denmark, from 1987 to 1988. From 1988 to 1992, he got the PhD degree in Electrical Engineering at Aalborg University in 1995. He became an Assistant Professor in 1992, an Associate Professor in 1996, and a Full Professor of power electronics and drives in 1998. From 2017 he became a Villum Investigator. He is honoris causa at University Politehnica Timisoara (UPT), Romania and Tallinn Technical University (TTU) in Estonia.
His current research interests include power electronics and its applications such as in wind turbines, PV systems, reliability, harmonics and adjustable speed drives. He has published more than 600 journal papers in the fields of power electronics and its applications. He is the co-author of four monographs and editor of ten books in power electronics and its applications.
He has received 31 IEEE Prize Paper Awards, the IEEE PELS Distinguished Service Award in 2009, the EPE-PEMC Council Award in 2010, the IEEE William E. Newell Power Electronics Award 2014, the Villum Kann Rasmussen Research Award 2014 and the Global Energy Prize in 2019. He was the Editor-in-Chief of the IEEE TRANSACTIONS ON POWER ELECTRONICS from 2006 to 2012. He has been Distinguished Lecturer for the IEEE Power Electronics Society from 2005 to 2007 and for the IEEE Industry Applications Society from 2010 to 2011 as well as 2017 to 2018. In 2019-2020 he serves a President of IEEE Power Electronics Society. He is Vice-President of the Danish Academy of Technical Sciences too. He is nominated in 2014-2018 by Thomson Reuters to be between the most 250 cited researchers in Engineering in the world.